BUTTERWORTH HEINEMANN

Parabolic numerical method for investigating free surface flows

S. R. Cakmakci and W. L. Hankey
Department of Mechanical and Materials Engineering, Wright State University, Dayton, OH, USA

Although one-dimensional analysis is a classical, accepted method used extensively in the literature and has been commonly used for the comparison with approximation methods for the solution of free surface flows, the requirement to specify the skin friction coefficient value has always been a constraint with which previous investigators have had trouble. The alternative method of solving the full Navier–Stokes equations requires substantial computer time because of the iteration necessary to resolve the location of the free surface boundary. A relatively simple parabolic numerical method for the thin-layer equations in two dimensions to solve the free surface flows without the need of assuming the skin friction coefficient and the need of iterating the free surface boundary is the purpose of this investigation. An order-of-magnitude analysis is used to reduce the elliptic governing Navier–Stokes equations to a parabolized set for high Reynolds numbers. The resulting equations are discretized and solved numerically for different sub and supercritical flows, various Pr, Fr, and Re numbers and for many different thermal boundary conditions using an implicit marching method employing the tridiagonal algorithm.

Keywords: thin layer; free surface boundary; skin friction coefficient; parabolic method

Introduction

Free surface flow refers to the flow of liquid wherein a portion of the uppermost boundary of the flow called the free surface is subject to atmospheric pressure. The movement of oceans, rivers, and irrigation systems, as well as the flow of liquids in partially filled pipes, and flows in canals are all examples of free surface flows. The forces causing flow are attributable to gravity, surface tension, and the forces retarding flow are attributable to viscous shear. Thus, the Weber number, the Froude number, and the Reynolds number are involved. When flow occurs at low velocities so that a small disturbance can travel against the flow and thus effect the conditions upstream, it is said to be subcritical flow ($Fr < 1$). If, on the other hand, the velocity of the stream is so high that a small disturbance, such as an elementary wave, is washed downstream, the flow is controlled by upstream conditions and is described as supercritical ($Fr > 1$). When flow velocity is just equal to the elementary wave velocity, the flow is called critical ($Fr = 1$).

The complete solutions of free surface flows are usually difficult to obtain because of the variable geometrical conditions and the state of the boundary surfaces. Therefore, a choice of a suitable friction factor is likely to be very uncertain.

Two general approaches are used for analyzing free surface flows: (1) the Navier–Stokes method, which is elliptic and requires at least an order of magnitude greater computer time than the parabolic method used in this paper; and (2) the one-dimensional method (Potter and Wiggert), which is rapid but requires specification of the skin friction that could be constant or vary as a function of axial distance.

For two-dimensional (2-D) free surface flows, numerical methods have been used by a number of investigators. Kothe and Mjolsness (1992), developed a numerical method for incompressible flows with free surfaces having significant surface tension forces. Jimenéz and Chaudhry (1988) solved the supercritical free surface flows by explicit numerical methods. Fennema and Chaudhry (1990) studied the explicit numerical methods for 2-D free surface flows. Rahman et al., (1990a, 1990b) solved the full Navier–Stokes equations by iterating the free surface boundary of free surface flows.

The brief literature survey presented in the foregoing reveals no parabolized numerical method to solve the free surface flows without requiring excessive computer time, or the skin friction coefficient, which is the purpose of this investigation.

A method is developed in this paper that determines the skin friction value intrinsically but saves over an order of magnitude in computer time compared to solving the complete Navier–Stokes equations. The method involves a parabolic procedure for the thin-layer equations describing free surface flows. This approach is analogous to parabolized Navier–Stokes equations (PNS), which are popular in the aerospace industry and used to solve compressible supersonic flows (Hankey, 1983). The Space Shuttle and the Aerospace Plane programs have exploited the use of PNS. The approach herein adopts this concept to solve difficult free surface flows.

The 2-D free surface flows for the steady laminar flow of a viscous incompressible fluid with heat transfer have been

Address reprint requests to S. R. Cakmakci, Sunset Ridge Apartments, #19, 1695 Kenneth Rd., York, PA 17404, USA.

Received 29 July 1994; accepted 31 March 1995

Int. J. Heat and Fluid Flow 16: 178–185, 1995

655 Avenue of the Americas, New York, NY 10010

0142-727X/95/$10.00
SSDI 0142-727X(95)00026-M

analyzed for both subcritical and supercritical flow conditions. Typical applications of this proposed parabolized solver for the thin-layer problems are for liquid cooling of elements used in coating processes, drying of different materials, gas absorption processes, and condensation processes.

Mathematical modeling of the hydrodynamical problem

The 2-D (x, y) governing equations of continuity and momentum for the laminar steady flow of Newtonian fluid with constant properties (dynamic viscosity μ, and density ρ are constants), without a velocity component in the z-direction ($w = 0$), and without the body forces in x and z directions in rectangular coordinates, with the assumption that the velocity film thickness $h(x)$ is very thin compared with the radial distance x; i.e., $x \gg h(x)$ as a result of the order-of-magnitude analysis are as follows:

Continuity:

$$\frac{\partial u}{\partial x} + \frac{\partial v}{\partial y} = 0 \tag{1}$$

x-Momentum:

$$u\frac{\partial u}{\partial x} + v\frac{\partial u}{\partial y} = -gh_x + \nu\frac{\partial^2 u}{\partial y^2} \tag{2}$$

The boundary conditions are as follows:

(1) No slip at wall; i.e., at $y = 0$; $u = v = 0$
(2) $y = h(x)$; $u = u_e(x)$

At the free surface $y = h(x)$, the effects of interfacial shear stress and the surface tension are assumed to be zero, although these can simply be added if desired.

To determine the pressure field for the problem, the y-momentum equation is integrated with respect to y, and applying the free surface boundary conditions the pressure field becomes the following:

$$P = -\rho g y + P_\infty + \rho g h(x) + 2\mu\frac{\partial v}{\partial y} \tag{3}$$

The following transformation of independent variables converts the original domain or physical plane into a rectangular region or computational plane (Hankey and Holden, 1975):

$$\xi = \int j\,dx, \qquad j = 1/h_{in}, \qquad \eta = y/h(x) \tag{4}$$

$$F(\xi, \eta) = u/u_e \tag{5}$$

where u_e = x-component of edge surface velocity; P_∞ = atmospheric pressure (static part); $2\mu\partial v/\partial y$ = viscous normal stress; $\rho g(h(x) - y)$ = potential component of the pressure field; h = velocity film thickness as a function of radial distance x; and h_{in} = constant inlet film thickness.

By using the transformations, it is now possible to apply finite differences on a uniformly spaced grid in the computational plane with the boundaries coinciding with the lines $\eta = 0$ and $\eta = 1$. To do this, the governing equations (Equations 1 and 2) are transformed in terms of ξ and η by applying the chain rule of partial differentiation. Then, the resulting thin layer equations are cast in conservation form in order to apply numerical schemes.

Thus, the governing equations become as follows:

$$v_\eta = (1/\eta_y)[u_e n_x F_n + \xi_x (u_e F)_\xi] \tag{6}$$

$$F_{\eta\eta} - VF_\eta - \beta F^2 = \gamma + 2\psi F F_\xi \tag{7}$$

where

$$V = (h/v)(v - u_e F \eta h_x) \tag{8}$$

$$\beta = (jh^2/v)u_{e_\xi} \tag{9}$$

$$\Upsilon = (jh^2 g h_\xi / v u_e) \tag{10}$$

$$2\psi = (jh^2 u_e / v) \tag{11}$$

By taking the derivative of Equation 8 with respect to η and combining with Equation 6

$$V_\eta + \sigma F = -2\psi F_\xi \tag{12}$$

where $\sigma = jh(hu_e)_\xi/v$, and β, ψ, and γ are the functions of ξ.

By defining Froude number based on the edge velocity $\mathrm{Fr}_e = u_e/(gh)^{1/2}$, the relationship between the σ, β, and Υ is

Notation

A	dimensionless temperature gradient
$F(\xi, \eta)$	dimensionless velocity
Fr	Froude number
g	gravitational acceleration
G	dimensionless temperature
h	velocity film thickness
h_t	thermal film thickness
j	transformation function
k	thermal conductivity
Nu	local Nusselt number
P	pressure
Pr	Prandtl number
Q	volume flow rate per unit width
Re	Reynolds number
T	temperature
u	component of velocity in x direction
v	component of velocity in y direction
w	component of velocity in w direction

Greek

α_t	thermal diffusivity
Δ	dimensionless film height
$\Delta\eta$	increment in η direction
$\Delta\xi$	increment in ξ direction
η	dimensionless function
μ	dynamic viscosity
ν	kinematic viscosity
ξ	dimensionless horizontal distance
ρ	density

Subscripts

e	edge
in	condition at entrance
m	node location in x direction
n	node location in y direction
sat	saturation
w	condition on solid wall
∞	atmospheric

obtained as

$$\sigma = \beta + \gamma\,\mathrm{Fr}_e^2 \tag{13}$$

The boundary conditions become

(1) $\eta = 0$; $F = 0$, $V = 0$
(2) $\eta = 1$; $F = 1$, $F_\eta = 0$, $V_e = 0$

where the subscript e stands for "the edge of" free surface, and the subscripts $\eta\eta$, η, ξ, x, and y denote the derivatives.

Integrating Equation 12 at the free surface by using the relationship of $h_x = v_e/u_e$ gives the following:

$$\sigma = -2\psi \frac{\int_0^1 F_\xi \,\mathrm{d}\eta}{\int_0^1 F \,\mathrm{d}\eta} \tag{14}$$

Integrating Equation 7 by using Equation 12, and the definitions of β and σ with the boundary conditions, and recollecting terms Υ can be rewritten as follows:

$$\Upsilon = \frac{2\sigma\int_0^1 F^2\,\mathrm{d}\eta + 4\psi\int_0^1 FF_\xi\,\mathrm{d}\eta + F_\eta(\eta = 0)}{1 - \mathrm{Fr}_e^2\int_0^1 F^2\,\mathrm{d}\eta} \tag{15}$$

In addition, an initial condition at $x = 0$; i.e., $(\xi = 0)$ is required for u. The arbitrary condition selected for this case is $F_\xi = 0$, or an initial similarity start. Obviously, other initial conditions may be explored.

For the similarity solution at the inlet, F is only a function of η, and σ, β, and Υ are all constants; therefore, the general free surface flow solutions (Equations 7 and 12) reduce to

$$F_{\eta\eta} - VF_\eta - \beta F^2 = \Upsilon \tag{16}$$

and

$$V_\eta + \sigma F = 0 \tag{17}$$

Finally, the constant volumetric flow rate per unit width perpendicular to the flow plane Q becomes the following:

$$Q = \int_0^h u\,\mathrm{d}y = u_e h\int_0^1 F\,\mathrm{d}\eta \tag{18}$$

Mathematical modeling of the thermodynamic problem

To determine the thermal distribution it is necessary to solve the equation resulting from the substitution of the solution of the hydrodynamic problem into the energy equation. By using the same assumptions as used for the hydrodynamical part of the problem, and implementing the order-of-magnitude analysis, the governing equation of energy for the laminar flow of a Newtonian fluid with constant properties (thermal conductivity k = constant, density ρ = constant) in rectangular coordinates is

Energy

$$u\frac{\partial T}{\partial x} + v\frac{\partial T}{\partial y} = \alpha_t\frac{\partial^2 T}{\partial y^2} \tag{19}$$

It is assumed that both the velocity film thickness h and thermal film thickness h_t are very thin compared with the radial distance x.

A dimensionless function G is introduced

$$G = \frac{T - T_w}{T_e - T_w} \tag{20}$$

with the boundary conditions

(1) $y = 0$, $T = T_w$, $G = 0$
(2) $y = h(x)$, $T = T_e$, $G = 1$

where T_w is the wall temperature; T_e is the temperature at the edge of the free surface; and both T_w and T_e are functions of radial distance x only.

By using Equations 4, 5, 8, 11, and 20, the energy equation is nondimensionalized as follows:

$$G_{\eta\eta} - \mathrm{Pr}VG_\eta = 2\psi\,\mathrm{Pr}\,F(G_\xi + AG + B) \tag{21}$$

where

$$A = \frac{(T_e - T_w)_\xi}{T_e - T_w} = \frac{\gamma\mathrm{Fr}_e^2}{2\psi} + \frac{q_{w_\xi}}{q_w} - \frac{G_{\eta\xi}(\eta = 0)}{G_\eta(\eta = 0)} \tag{22}$$

$$B = \frac{T_w}{T_e - T_w} \tag{23}$$

Pr is the Prandtl number, and A and B are dimensionless temperature gradients. Integrating Equation 21 by using Equation 12 with the boundary conditions and recollecting terms

$$G_\eta(\eta = 1) - G_\eta(\eta = 0) = \mathrm{Pr}\int_0^1 [(\sigma + 2\psi A)FG + 2\psi(FG)_\xi + 2\psi BF]\,\mathrm{d}\eta \tag{24}$$

The Nusselt number Nu_h in terms of film thickness is as follows

$$\mathrm{Nu}_h = G_\eta(\eta = 0) \tag{25}$$

To demonstrate the versatility of the method, an assortment of different boundary conditions are examined.

The boundary conditions are assumed to be: A) the same as the equilibrium temperature corresponding to the ambient vapor pressure (evaporation case) at the free surface with A1) constant wall temperature, A2) adiabatic wall surface, A3) uniform heat flux on the wall, and A4) constant Nusselt number; B) adiabatic free surface condition or heating case with B1) constant wall temperature, B2) uniform heat flux on the wall, and B3) constant Nusselt number.

Also, an initial upstream condition $T(0, y)$ is required to start the calculation. An arbitrary condition of $G_\xi = 0$, or an initial similarity start was selected. Obviously, other initial conditions can be explored.

Table 1 summarizes the boundary conditions.

Numerical solution of the hydrodynamical problem

To apply finite-difference methods, a finite-difference mesh in the ξ–η plane is considered (Figure 1). The values of the dependent variables at a grid point are identified by subscripts m and n to indicate positions along the ξ- and η-directions, respectively.

The derivations in Equation 7 are replaced by the central-difference approximations in the η-direction and backward-difference approximations in the ξ-direction. Rewriting the thin-layer nondimensional x-momentum (Equation

Table 1 Boundary conditions

At the free surface $\eta = 1$:

Evaporation $T_e = T_{sat} = \text{constant}$, $G = 1$

Heating $\partial T/\partial Y = 0$, $G_\eta = 0$

At the wall $\eta = 0$:

1) Constant wall temperature: $T = T_w = \text{constant}$, $G = 0$

Evaporation $A = B = 0$, $G_{\eta\eta} - \mathrm{Pr}VG_\eta = 2\psi \mathrm{Pr}FG_\xi$

$$G_\eta(\eta = 1) - G_\eta(\eta = 0) = \mathrm{Pr}\sigma \int_0^1 FG\,d\eta + 2\psi\mathrm{Pr}\int_0^1 (FG)_\xi\,d\eta$$

Heating $A = T_{e\xi}/(T_e - T_w)$, $B = 0$, $G_{\eta\eta} - \mathrm{Pr}VG_\eta = 2\psi\mathrm{Pr}F(G_\xi + AG)$

$$-G_\eta(\eta = 0) = \mathrm{Pr}\sigma\int_0^1 FG\,d\eta + 2\psi\mathrm{Pr}\left[A\int_0^1 FG\,d\eta + \int_0^1 (FG)_\xi\,d\eta\right]$$

2) Adiabatic wall surface: $\partial T/\partial Y = 0$, $G_\eta = 0$

Evaporation $A = -T_{w\xi}/(T_e - T_w)$, $B = -A$, $G_{\eta\eta} - \mathrm{Pr}VG_\eta = 2\psi\mathrm{Pr}F(G_\xi + AG - A)$

$$G_\eta(\eta = 1) = \mathrm{Pr}\sigma\int_0^1 FG\,d\eta + 2\psi\mathrm{Pr}\left[A\int_0^1 FG\,d\eta + \int_0^1 (FG)_\xi\,d\eta - A\int_0^1 F\,d\eta\right]$$

3) Constant wall heat flux: $-k\partial T/\partial Y = q_w = \text{constant}$, $(q_{w\xi} = 0)$

Evaporation $A = -T_{w\xi}/(T_e - T_w) = \gamma\mathrm{Fr}_e^2/2\psi - G_{\eta\xi}(\eta = 0)/G_\eta(\eta = 0)$, $B = -A$

$$G_\eta(\eta = 1) - G_\eta(\eta = 0) = \mathrm{Pr}\sigma\int_0^1 FG\,d\eta + 2\psi\mathrm{Pr}\left[A\int_0^1 FG\,d\eta + \int_0^1 (FG)_\xi\,d\eta - A\int_0^1 F\,d\eta\right]$$

Heating $A = (T_e - T_w)_\xi/(T_e - T_w) = \gamma\mathrm{Fr}_e^2/2\psi - G_{\eta\xi}(\eta = 0)/G_\eta(\eta = 0)$

$$-G_\eta(\eta = 0) = \mathrm{Pr}\sigma\int_0^1 FG\,d\eta + 2\psi\mathrm{Pr}\left[A\int_0^1 FG\,d\eta + \int_0^1 (FG)_\xi\,d\eta - B\int_0^1 F\,d\eta\right]$$

4) Constant Nusselt number: $\mathrm{Nu}_h = \text{constant}$, $(G_{\eta\xi}(\eta = 0) = 0)$

Evaporation $A = -T_{w\xi}/(T_e - T_w) = \gamma\mathrm{Fr}_e^2/2\psi + q_{w\xi}/q_w$, $B = -A$

$$G_\eta(\eta = 1) - G_\eta(\eta = 0) = \mathrm{Pr}\sigma\int_0^1 FG\,d\eta + 2\psi\mathrm{Pr}\left[A\int_0^1 FG\,d\eta + \int_0^1 (FG)_\xi\,d\eta - A\int_0^1 F\,d\eta\right]$$

Heating

$$-G_\eta(\eta = 0) = \mathrm{Pr}\sigma\int_0^1 FG\,d\eta + 2\psi\mathrm{Pr}\left[A\int_0^1 FG\,d\eta + \int_0^1 (FG)_\xi\,d\eta - B\int_0^1 F\,d\eta\right]$$

where T_{sat} is the saturation temperature, and q_w is the wall heat flux.

7) in the finite-difference form and rearranging (Cheney and Kincaid, 1985)

$$F_{m,n} = e_{m,n}F_{m,n+1} + w_{m,n} \tag{26}$$

where

$$a_{m,n} = 1 - \frac{V_{m,n}\Delta\eta}{2}$$

$$b_{m,n} = 2 + \beta_m F_{m,n}\Delta\eta^2 + \frac{2\psi_m\Delta\eta^2 F_{m,n}}{\Delta\xi}$$

$$c_{m,n} = 1 + \frac{V_{m,n}\Delta\eta}{2}$$

$$d_{m,n} = \left[\frac{2\psi_m F_{m,n}F_{m-1,n}}{\Delta\xi} - \gamma_m\right]\Delta\eta^2$$

$$e_{m,n} = \frac{a_{m,n}}{b_{m,n} - c_{m,n}e_{m,n-1}}$$

$$w_{m,n} = \frac{d_{m,n} + c_{m,n}w_{m,n-1}}{b_{m,n} - c_{m,n}e_{m,n-1}}$$

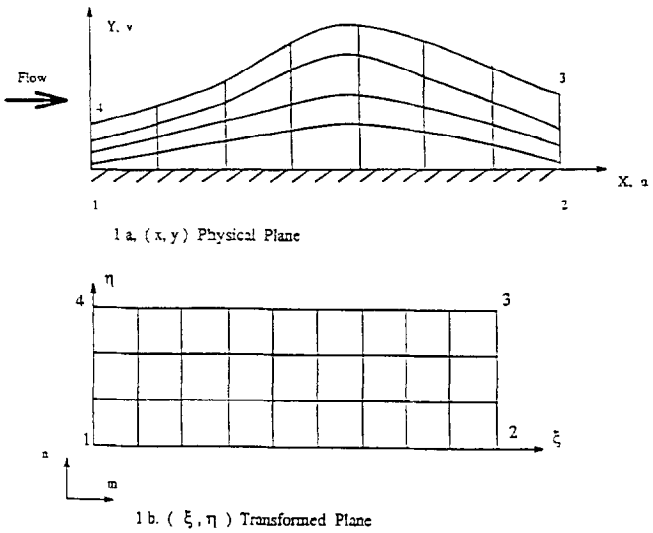

Figure 1 Physical and transformed planes of the problem under consideration

$\Delta\xi$ and $\Delta\eta$ are the step size increments in ξ and η directions respectively. The individual sets of equations form a tridiagonal matrix (Roache, 1976) and are solved using the simple Thomas algorithm, which factorizes the matrix into two triangular matrices (by assuming a linear relationship) and uses forward and backward substitution.

The computation starts first calculating $a_{m,n}$, $b_{m,n}$, $c_{m,n}$, $d_{m,n}$, $e_{m,n}$, and $w_{m,n}$ at the wall and continues through the free surface. The solution sweeps back from the free surface to the wall boundary condition by calculating the velocity vector $\mathbf{F}_{m,n}$ by the recursion relationship of Equation 26. The flow field is solved simultaneously with the film thickness, Froude number, and Reynolds number in the radial direction. Therefore, the solution technique is an implicit parabolic marching method starting from the inlet condition where an initial thin film is generated and enters the control volume, to where it continues depending upon the Froude number.

The marching in the dimensionless horizontal distance ($\xi = x/h_{in}$) starts at the inlet by using the initial Froude number, Reynolds number, and a guessed velocity field. The inlet conditions denoted by a subscript $m = 1$ are given by

$$F_{\xi 1} = 0,\ 2\Psi_1 = \mathrm{Re}_{h1},\ \sigma_1 = 0,\ \beta_1 = -\gamma_1 \mathrm{Fr}_{e1}^2 \cdot V_{1,n} = 0 \quad \text{and}$$

$$\gamma_1 = -\frac{F_\eta(\eta = 0)}{1 - \mathrm{Fr}_{e1}^2 \int_0^1 F^2\, \mathrm{d}\eta}$$

where the Reynolds number is defined based on the film thickness h; i.e., $\mathrm{Re}_h = hu_e/\nu$.

After the velocity field convergence is achieved, the new values of 2ψ, β, σ, and γ are calculated from Equations 11, 13, 14, and 15, respectively, which are then to be used for the next downstream location.

The new dimensionless film thickness Δ_m, Reynolds number Re_{hm}, and Froude number Fr_{em} as $m = 2, 3, 4, \ldots, j, j+1$ are calculated along the radial direction, and given by

$$\Delta_m = (h/h_{in})_m = [\Upsilon_m \mathrm{Fr}_{em}^2/Re_{hm}]\Delta\xi + \Delta_{m-1}$$

$$\mathrm{Fr}_{em}^2 = \mathrm{Re}_{hm}^2 \mathrm{Fr}_{e1}^2/\mathrm{Re}_{h1}^2 \Delta_m^3$$

$$\mathrm{Re}_{hm} = \sigma_m \Delta\xi/\Delta_m + \mathrm{Re}_{hm-1}$$

The procedure stops when an average $\mathrm{Fr} = 1$ is achieved at the critical state. The marching parabolic method cannot pass through critical.

Numerical solution of the thermodynamic problem

The same numerical method is applied as for the hydrodynamical problem to solve the temperature profile. The derivatives in thin-layer Equation 21 are replaced by the central-difference approximations in η-direction and backward-difference approximations in ξ-direction to be defined in the Thomas algorithm (Roache, 1976).

Rewriting the nondimensional energy equation in the finite-difference form and rearranging

$$G_{m,n} = e'_{m,n} G_{m,n+1} + w'_{m,n} \tag{27}$$

where

$$a'_{m,n} = 1 - \frac{\mathrm{Pr} V_{m,n} \Delta\eta}{2}$$

$$b'_{m,n} = 2 + 2\psi_m \mathrm{Pr} A F_{m,n} \Delta\eta^2 + \frac{2\psi_m \mathrm{Pr} \Delta\eta^2 F_{m,n}}{\Delta\xi}$$

$$c'_{m,n} = 1 + \frac{\mathrm{Pr} V_{m,n} \Delta\eta}{2}$$

$$d'_{m,n} = 2\psi_m \mathrm{Pr} F_{m,n} \Delta\eta^2 \left(\frac{G_{m-1,n}}{\Delta\xi} - B \right)$$

$$e'_{m,n} = \frac{a'_{m,n}}{b'_{m,n} - c'_{m,n} e'_{m,n-1}}$$

$$w'_{m,n} = \frac{d'_{m,n} + c'_{m,n} w'_{m,n-1}}{b_{m,n} - c_{m,n} e'_{m,n-1}}$$

The computation starts first calculating $a'_{m,n}$, $b'_{m,n}$, $c'_{m,n}$, $d'_{m,n}$, $e'_{m,n}$, and $w'_{m,n}$ at the wall at each m station and then the value of A, which satisfies the boundary conditions, is calculated by the bisection or half-interval method (Cheney, 1985). For all the boundary conditions, the starting value for A at the initial station $m = 1$ is zero or $G_\xi(\xi = 0) = 0$ condition. Afterward, the computation continues through the free surface by incorporating the previously calculated velocity field. Then, the values of $G_{m,n}$ are computed inwardly from the free surface to the wall boundary.

For both the evaporation and heating with constant wall heat flux case, at the first station ($m = 1$) any trial value of $G_\eta(0)$ is guessed, and the corresponding A value is computed to ensure that $G_\xi(\xi = 0) = 0$. At the subsequent stations, both variable $G_\eta(0)$ and A are computed.

The wall boundary value of $G_\eta(0)$ is a fixed value for the constant Nusselt number, zero for the adiabatic wall surface, and variable for the constant wall heat flux case. An initial $G_{m,n}$ profile is assumed for the heating with constant Nusselt number, and the constant wall heat flux, and every m station two loops one for the convergence of B, and one for the convergence of $G_\eta(\eta = 0)$ are employed.

The solution has more than one root for A. However, the stability criteria of the Thomas algorithm is not satisfied, except for the first root of A (Cakmakci, 1993).

Results and discussion

The parabolized thin-layer equations (Equations 7 and 21) describing free surface flows with their corresponding boundary conditions have been solved by an implicit marching method employing the tridiagonal algorithm for four inlet Reynolds numbers (100, 1000, 5000, 10000) and five inlet Froude numbers (0.2, 5.0, 10.0, 15.0, 20.0). The results are given in Figures 2–10.

The Froude number profiles for subcritical and supercritical flows are shown in Figures 2 and 3. As the Froude number

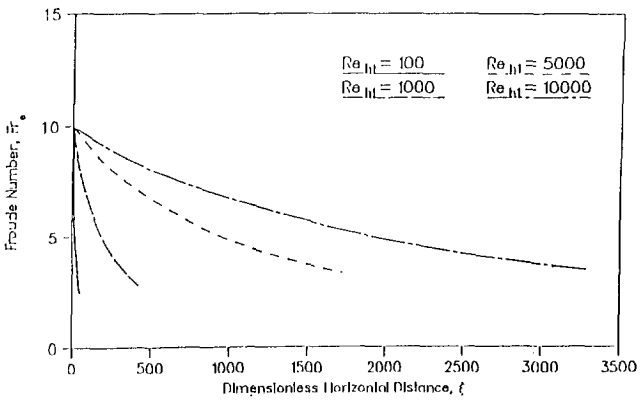

Figure 2 Froude number profile for supercritical flows with $\mathrm{Fr}_{e1} = 10$

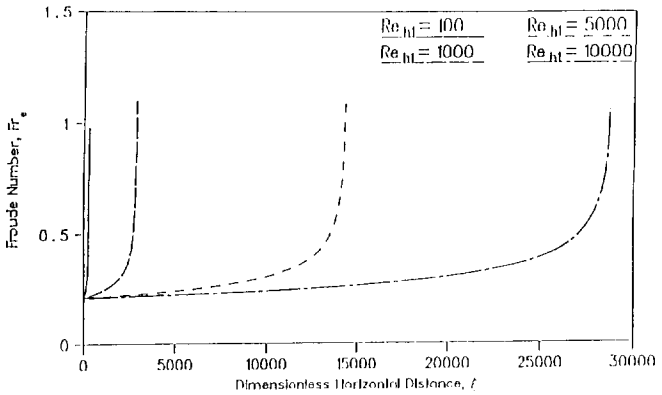

Figure 3 Froude number profile for subcritical flows with $Fr_{e1} = 0.2$

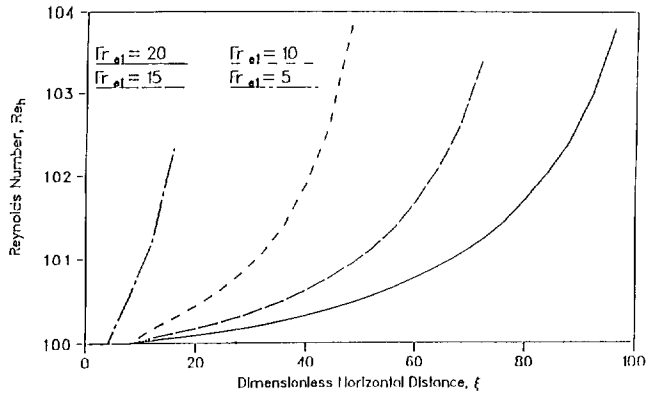

Figure 4 Reynolds number profile for supercritical flows with $Re_{h1} = 100$

becomes smaller for subcritical flows or becomes larger for supercritical flows, it takes a longer distance to reach the critical Froude number (Fr = 1). All flows may be computed up to the critical state where a singularity exists and cannot pass through Fr = 1.

The Reynolds number profiles for supercritical flows are shown in Figure 4. As the gravitational forces decrease, or Froude number increases, the velocity of the fluid increases, in turn.

The effects of changing the inlet Reynolds number and the inlet Froude number on the film height are presented in Figures 5 and 6 for both subcritical and supercritical flows. By increasing the inlet Reynolds number, the subcritical and supercritical solutions can be sustained for larger distances because of the bigger inertial forces. The increase in the fluid velocity is correlated to an increasing viscous force, which translates into an increase in the film thickness with distance through the continuity equation in the supercritical region. However, because of friction, film thickness decreases with distance in the subcritical region. When the inlet Froude number is high, the flow can maintain its supercritical status for a longer distance because of the lower gravitational forces. In the case of zero gravity, the flow stays entirely supercritical, and a subcritical flow regime becomes impossible. On the contrary, decreasing the inlet Froude number while the inlet Reynolds number remains constant causes a longer subcritical status because of the higher amount of gravitational forces.

Comparing the results of the flow analysis with the one-dimensional Chezy–Manning equation (Potter and Wiggert, 1991) there is less than 2% difference for subcritical flows and less than 3% difference for supercritical flows, as shown in Figures 5 and 6.

The heat transfer behavior (Equation 21) was solved by incorporating the momentum equation in the solution algorithm, for an inlet Reynolds number of 100, and two inlet Froude numbers (0.2 and 10) with Prandtl number of 7. The results are given in Figures 7–10.

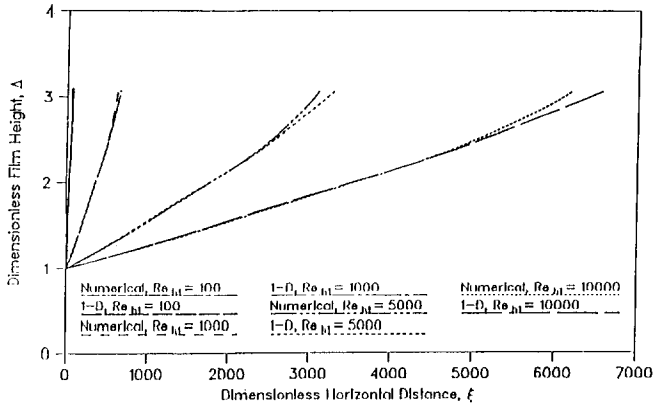

Figure 5 Comparison of film height profile for supercritical flows with $Fr_{e1} = 10$

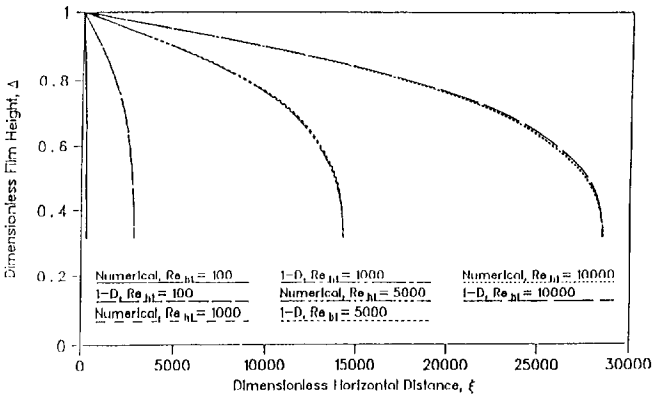

Figure 6 Comparison of film height profile for subcritical flows with $Fr_{e1} = 0.2$

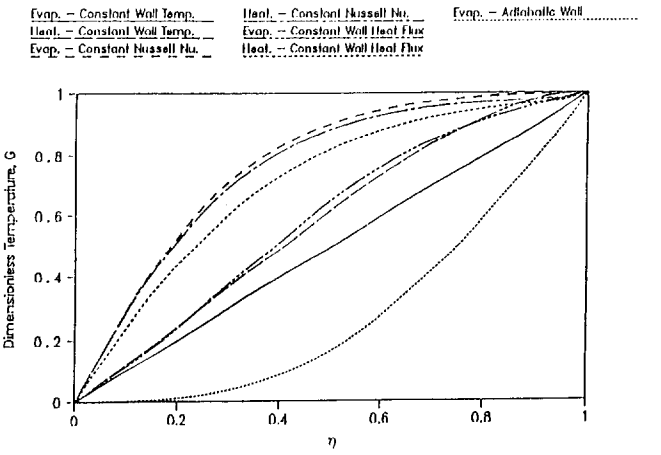

Figure 7 Dimensionless temperature profiles for subcritical flows with $Fr_{e1} = 0.2$

The dimensionless temperature profiles for the evaporation and heating cases are shown in Figures 7 and 8. The profiles appear to be similar for subcritical and supercritical cases, which are parabolic in nature and linear for evaporation constant wall temperature cases.

Comparing the results of the heat transfer analysis with the analytical solution, the temperature distribution was expected to be linear for the evaporation constant wall temperature, and Figures 7 and 8 show that fact (Cakmakci, 1993).

The distributions of the Nusselt number for the subcritical and supercritical cases are shown in Figures 9 and 10. The Nusselt number considered for the problem depends upon two parameters; namely, the film height and the heat transfer coefficient. Nusselt number remains approximately uniform for an isothermal surface as an indication of a stable thermal thin-layer thickness. In the subcritical region, there is a sudden drop of the Nusselt number near the entrance for constant wall heat flux surface, and decreases gradually downstream when there is evaporation, but decreases monotonically for the heating case. The heat transfer coefficient decreases with the growth of the thermal thin layer causing more resistance to heat transfer from the wall. For the heating case, because the free surface is adiabatic in nature, there is a much slower decrease in the heat transfer coefficient than the evaporation case. Although the film height decreases with the distance in the subcritical regime, the thermal layer increases, causing the drop of the Nusselt number. This phenomenon can only be explained by the fact that the solutions are for the fully developed region where the Reynolds numbers are high, and the entire film thickness is engulfed by the thermal thin layer. In the supercritical region, the behavior of the Nusselt number is analogous to the subcritical flow except near the entrance. The decrease of the Nusselt number is not sudden but gradual.

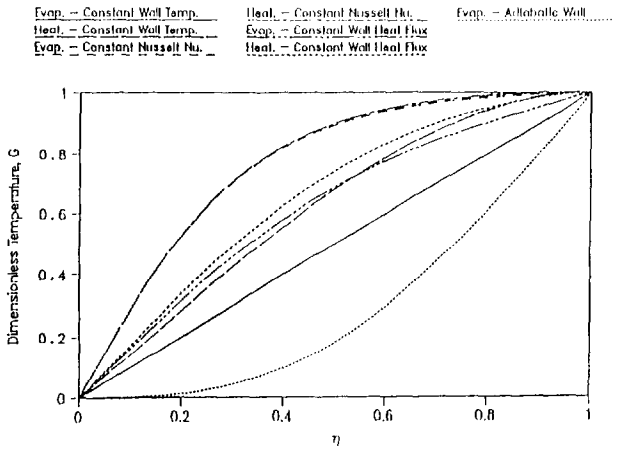

Figure 8 Dimensionless temperature profiles for supercritical flows with $Fr_{e1} = 10$

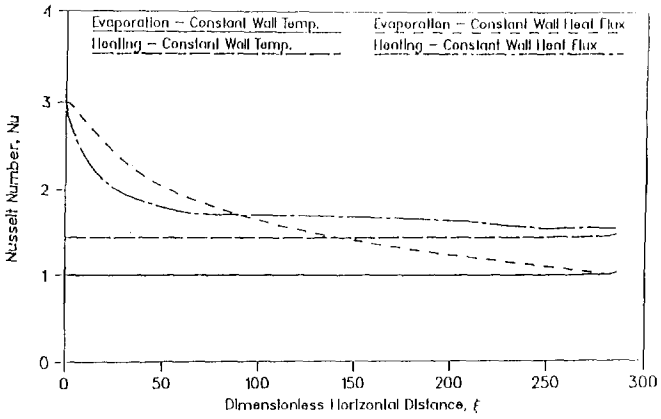

Figure 9 Nusselt number profiles for subcritical flows with $Fr_{e1} = 0.2$

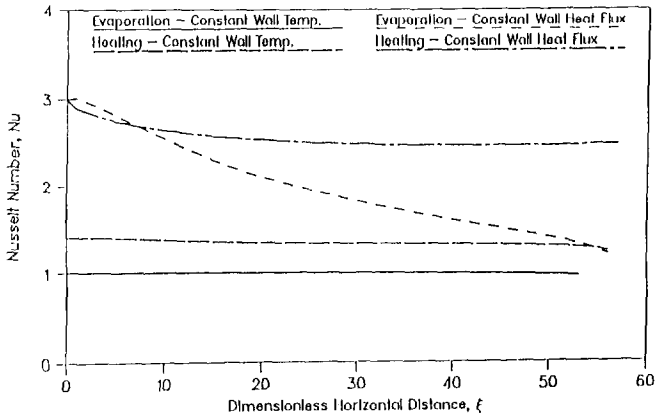

Figure 10 Nusselt number profiles for supercritical flows with $Fr_{e1} = 10$

Finally, although this problem was solved for the incompressible fluid, a similar approach used for the solution of the compressible boundary layer equations (Hankey and Holden, 1975) can be applied for variable density free surface flows. Variable density requires coupling of energy equation with momentum equation and adds an iteration.

Conclusion

Free surface flows wherein a portion of the uppermost boundary of the flow is subject to no boundaries are commonly found during condensation on a solid surface in a heat exchanger or cooling tower, in metal industries, in irrigation systems, and film-cooling processes. Beyond practical applications, the mechanics of free surface flows is important from a theoretical point of view, because viscosity or skin friction, variable geometrical boundary conditions that make it harder to locate the free surface boundary, and free surface effects are significant in these flows. Therefore, understanding such flows is essential and is the primary motivation for the present study.

A numerical parabolic method for the computation of thin-layer equations describing free surface flows has been developed to eliminate the need for specifying the skin friction as in the one-dimensional method, and to reduce the computer time caused by the free surface boundary iteration, as in the solution of the full Navier–Stokes equations. The analysis is carried out in two parts. First, the hydrodynamics of the flow are studied where the skin friction value is determined intrinsically for 2-D flow of an incompressible fluid. Next, the thermodynamics of the same steady laminar flow are examined by incorporating the hydrodynamics of the problem for many different thermal boundary conditions.

An order-of-magnitude analysis is used for both the analysis of flow and heat transfer to reduce the governing equations to a parabolized set. The resulting equations are solved numerically by an implicit marching method employing the Thomas algorithm without the need to iterate the location of the free surface boundary. As a result, the solutions were obtained with at least one order-of-magnitude less computer time than the

elliptic Navier–Stokes method. The method successfully and rapidly solves a wide variety of problems for different sub- and supercritical flows.

References

Cakmakci, S. R. 1993. Analytic and numerical investigation of parabolic free surface flows. M.S. thesis, Wright State University, Dayton, OH

Cheney, W. and Kincaid, D. 1985. *Numerical Mathematics and Computing*. 2nd edn. Brooks/Cole Publishing Company, Pacific Grove, CA

Fennema, R. J. and Chaudhry, M. H. 1990. Explicit methods for 2-D transient free surface flows. *J. Hyd. Eng.*, **116**, 1013–1034

Hankey, W. L. 1983. *Introduction to Computational Aerodynamics*. Wright State University Press, Dayton, OH

Hankey, W. L. and Holden, M. S. 1975. Two-dimensional shock wave-boundary layer interactions in high-speed flows. *Advisory Group for Aerospace Research & Development*, **203**, 2–11

Jiménez, O. F. and Chaudhry, H. M. 1988. Computation of supercritical free surface flows. *J. Hyd. Eng.*, **114**, 377–395.

Kothe, D. B. and Mjolsness, R. C. 1992. RIPPLE: a new model for incompressible flows with free surfaces. *AIAA J.*, **30**, 2694–2700

Potter, M. C. and Wiggert, D. C. 1991. *Mechanics of Fluids*. Prentice-Hall, Englewood Cliffs, NJ

Rahman, M. M., Faghri, A., Hankey, W. L. and Swanson, T. D. 1990a. Computation of the free surface flow of a thin liquid film at zero and normal gravity. *Num. Heat Transfer*, **17A**, 53–71

Rahman, M. M., Faghri, A., Hankey, W. L. and Swanson, T. D. 1990b. Prediction of heat transfer to a thin liquid film in plane and radially spreading flows. *J. Heat Transfer*, **112**, 822–825

Roache, P. J. 1976. *Computational Fluid Dynamics*. Hermosa Publishers, NM